Global Journal of Pure and Applied Mathematics.
ISSN 0973-1768 Volume 19, Number 2 (2023), pp. 555-578

http://www.ripublication.com

Wind farm layout optimisation on complex terrain using the depth-averaged method

[1]Anna Avramenko, **[2]Jari Hamalainen**, **[3]Jiann-Fuh Chen,**

[1]School of Engineering Science, Lappeenranta-Lahti University of Technology, Lappeenranta, Finland,

2School of Engineering Science, Lappeenranta-Lahti University of Technology, Lappeenranta, Finland

Department of Electrical Engineering, National Cheng Kung University, Taiwan

Email Anna.Avramenko@lut.fi,

Abstract

As wind energy is increasingly exploited worldwide, new wind farms are located in challenging environments instead of flat terrain or offshore. Therefore, wind farm layout optimisation becomes more crucial. A simplified set of fluid-dynamical equations was derived for model-based optimisation purposes, with the model still being accurate enough for complex flows. The novel method is based on equations where the flow variables are averaged in the vertical direction, thus reducing dimensions from three to two and simultaneously cutting computational time drastically. This implies that only the bulk velocity is predicted by the resulting depth-averaged model, and the complex terrain is represented as source terms of the equations. The wind farm layout optimisation problem has been identified by using evolutionary algorithms to avoid difficulties in the gradient calculations of the objective function. The depth-averaged CFD model has been tested with the Lillgrund wind farm. While the model has been found to predict the wind velocity and power of the turbines with good accuracy, it is also computationally cheap when running optimisation applications. A case study based on a wind farm with five turbines on a Gaussian hill is presented to demonstrate the ability of this method. The results show that the algorithm can find a better design, with 4.6% higher total power than the original design, while keeping a minimal distance between the turbines and the occupied area.

Keywords wind farm layout optimisation, complex terrain, CFD, evolutionary programming, depth-averaged method.

Introduction

Many suitable sites are already well-developed with regard to wind farms on flat terrain. Now, more and more attention is being devoted to building wind farms on complex terrain, especially due to the mountainous terrain features. Compared to a wind farm built on flat terrain, a wind farm on complex terrain could gain the benefits of a possible richer wind resource at certain terrain topographies (obtained by the speed-up effect due to changes in landscape). However, it is also more likely to be exposed to higher fatigue loads and operation costs, complex flow conditions and installation, and other disadvantages (Feng et al. (2018)).

It is a non-trivial task to design wind farms on complex terrain, which is mainly due to the wind turbine wakes and the multidisciplinary nature of the wind farm design problem, as well as the complex interactions of the boundary layer flow with the terrain topography. This problem typically involves engineering tasks and different design, which may come from logistical, environmental, economic, technical and legal considerations.

Wind flow modelling over complex terrain has been investigated by many researchers for a very long time. In 1947, Queney (1947) gave a review of the theoretical models of inviscid flow over mountains and hills. In 2000, Wood (2000) published a review of studies on wind flow over complex terrain. The problems of wind resource assessment on complex terrain have also been investigated by many scientists for a long time (Landberg et al. (2003)).

Recently, the wind farm layout optimisation was considered by many researchers, although the majority of the published studies in this field have focused on the optimising layouts on uniform and flat terrain (Amarala and Castro (2017); Osuna-Enciso et al. (2018); Gonzalez et al. (2014); Turner et al. (2014); Park and Law (2015); Gao et al. (2014)). Several studies examined the wind farm layout optimisation problem on complex terrain.

Kuo et al. (2016) proposed an algorithm that combines mixed-integer programming (MIP) and computational fluid dynamics (CFD) for wind farm layout optimisation on complex terrains. The improvement of the accuracy of wake deficit predictions was produced by CFD simulations and the optimisation process was done by MIP. The described method was used on a wind farm on complex terrain in Carleton-sur-Mer, Quebec, Canada. The obtained data demonstrated that the proposed method could suggest good layouts on complex terrains.

Allen et al. (2019) modified NREL's WindSE RANS code for layout optimisation on complex terrain. WindSE is an open source CFD tool from the National Renewable Energy Laboratory (NREL). WindSE was accessible for the gradient-based optimising of wind farm layouts on uniform topography (King et al. (2017)). However, the modifications are able to include terrain effects such as wake curvature and flow separation. Two wind farm layout optimisation studies were performed. A simplified Gaussian hill was used in the first study to confirm that WindSE's automatic differentiation predicts well the terrain effects when calculating the gradients for optimisation. Nine wind turbines, four inflow directions and a skewed hill were

considered in the second layout study. The results show the significant power improvements over gridded layouts.

An optimisation framework comprising the results from WAsP CFD (wind resource assessment tools), an advanced optimisation algorithm and a fast engineering wake model, was developed by Feng et al. (2018). The performance of proposed algorithms and the effectiveness of the framework for wind farm layout optimisation were demonstrated on the real wind farm on complex terrain. The results demonstrated the 2.7% total net annual energy production of the wind farm increase using realistic constraints, such as minimal distance between turbines and the maximal terrain ruggedness index.

Automated model-based optimisation methods serve as tools when searching for optimal layouts, assuming that a mathematical model can accurately predict wind flows and the resulting wind energy productions. A model also needs to be fast enough to be integrated with optimisation algorithms to be solved hundreds or thousands of times. CFD is the most accurate prediction approach for wind flows in complex terrains, but, unfortunately, even one CFD simulation requires a long time for computing. In this paper, a layout optimisation on complex terrain using the CFD-based tool coupled with an evolutionary algorithm is presented. The required data on the flow behaviour over hills is extracted from depth-averaged RANS simulations, rather than from effective and analytical models. The main assumption of the presented method is that the terrain effects can be presented with the source terms in governing equations. Modelling the detailed geometry and generating a good-quality mesh is very time-consuming in 3D simulation. The actual 3D simulation of wind farms takes a lot of computational time. However, the modelling and discretisation of complex 3D geometry are not needed in the pre-processing state for the presented depth-averaged approach. Furthermore, the two-dimensional depth-averaged equations are solved in a fixed two-dimensional computational domain and the depth of an original domain appears only in the source terms of the equations.

The depth-averaged method was also used by Lyytikainen et al. (2009) in a fast modelling tool for plate heat exchangers. It was demonstrated that the depth-averaged model predicts the profile of the temperature change and pressure drop as a function of the corrugation length and angle with relatively good accuracy.

In addition, wind turbines are introduced as body forces by using the actuator disc approach. The obtained set of equations has been found to be accurate and fast, thus suitable for wind farm layout optimisation over complex terrains. The overall energy production of a wind farm is the objective function to be maximised by searching for the best wind turbine locations. The optimisation variables are the wind turbine horizontal (x,y) coordinates, which are subject to constraints for minimum distances between the turbines, and boundary conditions where the turbines can be located. The wind farm layout optimisation problem has been identified by using evolutionary algorithms to avoid difficulties in the gradient calculations of the objective function. The differential evolution was used to search the optimal result.

A comparison with the well-known Lillgrund wind farm indicates that the depthaveraged model is also able to determine the power of the various turbines, supporting its estimation procedure from the wind energy point of view, even though some of the 3D flow structures are lost. Finally, the obtained set of depth-averaged equations is used to optimise the layout of a farm over complex terrain, where a genetic search algorithm is used.

Methodology

The objective of this work is to present a novel method capable of integrating CFD simulation data for wind farm layout optimisation on complex terrains. In recent years, the wind energy community has demonstrated an increasing interest in using CFD models such as Reynolds-averaged Navier Stokes (RANS) models or large eddy simulations (LES) for the optimisation of wind farm layouts. These CFD models preserve more of the true flow physics by solving either the spatially filtered (in the case of LES) or the ensemble-averaged (in the case of RANS) Navier Stokes equations.

In recent years, RANS modelling has received particular attention in its handling of complex terrain and high dimensional optimisation (Allen et al. (2019)). A number of recent experimental and computational studies have examined wind turbine wakes in complex terrain. These studies have demonstrated the use of many different RANS turbulence models such as $\kappa - \varepsilon$ and $\kappa - \omega$ (Politis et al. (2012)), shown that RANS actuator disk models can compare favourably to LES with actuator lines (Sessarego et al. (2018)), and found generally good agreement between field experiments, wind tunnel experiments, and CFD (Conan et al. (2016)). RANS models are used in this study as they strike a balance between computational cost and fidelity while improving the prediction of time-averaged flow fields and power production.

However, using CFD-RANS simulation methods would lead to a months-long CPU time when coupled with mathematical optimisation. Hence, the development of faster modelling methods is needed for the real optimisation processes.

Integrating the standard RANS Navier-Stokes equations in the vertical direction, the depth-averaged 2D model has been derived with regard to the varying height of the channels. Depth-averaging was used in the derivation of open-channel flow models (Rastogi and Rodi (1978); Rodi (1984); Hamalainen et al. (2008)). The derivation is technically similar to the open channel problems, but other assumptions for the velocity and pressure profiles in the vertical direction are needed. Knowing the depth $D = D(x_1, x_2)$, the velocity profile in the vertical direction can be presented as

$$u_i(x_1, x_2, x_3) = U_i(x_1, x_2)S(x_3),$$

where the depth-averaged velocity is

$$U_i(x_1, x_2) = \frac{1}{D}\int_{d_1}^{d_2} u_i(x_1, x_2, x_3)\, dx_3,$$

and the profile is

$$S(x_3) = \frac{n+1}{n}\left(1 - \left|1 - \frac{1}{D}x_3\right|^n\right),$$

where $n = 7$ for turbulent flows.

Assuming the static pressure p is the constant in the vertical direction, the final equations are similar to the standard 2D equations, except the depth-averaged equations include new source terms due to the depth-averaging process:

$$\nabla \cdot \left(\rho \vec{U}\right) = -\frac{\rho}{D}\vec{U} \cdot \nabla D =: S_{mass},$$

$$\nabla \cdot \left(\rho \vec{U}\vec{U}\right) = -\nabla p + \nabla \cdot \bar{\bar{\tau}} + US_{mass} - \frac{8\mu U}{D^2} = -\nabla p + \nabla \cdot \bar{\bar{\tau}} + S_m,$$

The equations above indicate mass and momentum conservation laws, where p is the pressure, μ is the dynamic viscosity, ρ is the density, $\bar{\bar{\tau}}$ is the stress tensor, D is the channel's depth and $\vec{U}$ is the depth-averaged velocity vector. In addition to the mass balance and momentum equations already derived, the turbulence quantities also should be simulated. The $\kappa - \varepsilon$ model for depth-averaged modelling was presented by Rastogi and Rodi (1978); Rodi (1984) for open-channel flows:

$$U_1\frac{\partial k}{\partial x} + U_2\frac{\partial k}{\partial y} = \frac{\partial}{\partial x}\left(\frac{\nu_t}{\sigma_k}\frac{\partial k}{\partial x}\right) + \frac{\partial}{\partial y}\left(\frac{\nu_t}{\sigma_k}\frac{\partial k}{\partial y}\right) + P_h + P_{k\nu} - \epsilon,$$

$$U_1\frac{\partial \epsilon}{\partial x} + U_2\frac{\partial \epsilon}{\partial y} = \frac{\partial}{\partial x}\left(\frac{\nu_t}{\sigma_\epsilon}\frac{\partial \epsilon}{\partial x}\right) + \frac{\partial}{\partial y}\left(\frac{\nu_t}{\sigma_\epsilon}\frac{\partial \epsilon}{\partial y}\right) + c_{1\epsilon}\frac{\epsilon}{k}P_h + P_{\epsilon\nu} - c_{2\epsilon}\frac{\epsilon^2}{k},$$

The production of turbulent energy for $\kappa - \varepsilon$ equations is included via production terms

$$P_{k\nu} = \frac{c_k U_*^3}{D},$$

$$P_{\varepsilon\nu} = \frac{c_\varepsilon U_*^4}{D},$$

where the empirical constants are

$$\boldsymbol{c_k = \frac{1}{\sqrt{c_f}}},$$

$$\boldsymbol{c_\epsilon = 3.6\frac{c_{2\epsilon}}{c_f^{3/4}}\sqrt{c_\mu}},$$

$\boldsymbol{c_f}$ is the friction coefficient and $c_\mu = 0.09$, $c_{2\epsilon} = 1.92$ are standard constants for the $\kappa - \varepsilon$ model.

The derived equations can be applied for the open-channel flow modelling on complex terrain, but they do not include the wind turbines. While the flow around the turbine can be resolved exactly with reasonable accuracy, its high computational cost makes it unsuitable for optimisation of wind farm layouts. An alternative way for wind turbine flow modelling is to define the region of the actuator disk at the location of the turbine. In this case, the aerodynamic effect of rotating blades can be presented by the momentum transferred over thin disk with an area equal to the swept area of the rotor. The momentum may be added by defining a boundary condition at the location of the actuator disk or as a volume source. This method is particularly suited to 3D wind farm simulation on complex terrain. However, when it comes to depth-averaging the new approach is required.

The objective function of the wind farm layout optimisation problem is the power output of the wind farm:

$$\boldsymbol{P = \sum_{i=1}^{n} P_i},$$

where n is the number of turbines, P_i represents the power of each turbine:

$$\boldsymbol{P_i = \frac{\rho A C_p u^3}{2}},$$

Here, ρ is the density, A is the disk area, C_p is the power coefficient of the turbine and u is the velocity. All parameters for wind farm power calculation are well known except for the velocity. As a result, all flow characteristics such as turbulence quantities, pressure, etc. are important in general, but do not need to be modelled for the wind farm layout optimisation. Therefore, the main goal of the depth-averaged approach is to obtain the same velocity field as in 3D simulation.

In the presented model, only the mesh in x- and y-directions is available due to averaging in z-direction. Let us present the turbine as a line where its length is the diameter of the turbine (see Figure 1).

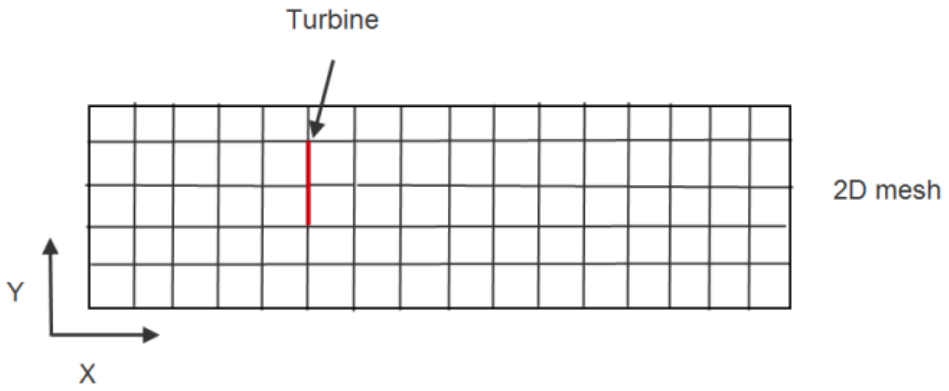

Figure 1. Wind turbine in 2D simulation.

The idea comes from the porous jump boundary conditions (Brillard (1987)). To simulate a thin porous medium where the velocity (pressure-drop) characteristics are known, porous jump conditions are applied. It is essentially a 1D simplification of the full porous media model available for cell zones. The turbine is included in the depthaveraged governing equations using user-defined functions (UDFs) as a source term, described by

$$\boldsymbol{\Delta p = \left(\frac{\mu}{\alpha} u + \frac{1}{2} C_2 \rho u^2\right) \Delta m},$$

where μ is fluid viscosity, α represents the permeability, C_2 is the inertial resistance factor, u is the velocity normal for the porous face and Δm is the thickness of the turbine. The unknown coefficients in this equation are permeability and the inertial resistance factor. Only these terms need to be evaluated in order to calculate the pressure drop.

According to the Actuator Disk theory, the coefficient $1/\alpha = 0$ (Avramenko (2019)). It is absolutely obvious that it is impossible to calculate the last parameter analytically. The only way to find the inertial resistance factor numerically is to compare the velocity field from 3D and 2D simulations for each kind of turbine. Although the depth-averaged approach requires preliminary calculations, they are needed only once to find the required parameter.

The effects of the hub height are included in the depth-averaged simulation by using the inertial resistance factor. It means that if the 3D simulations for the same wind turbines on different hub heights are executed, the velocity profiles are different due to the height of the turbine. Therefore, the inertial resistance factor in depth-averaged modelling is also changed for turbines with different hub heights.

A complete system of equations 1-5 provides the depth-averaged 2D method for wind farm simulation on complex terrain that is used together with the evolutionary

algorithm for wind farm layout optimisation. Evolutionary algorithms are optimisation methods that imitate the selection and evolution of nature. Figure 2 presents the general scheme of these algorithms.

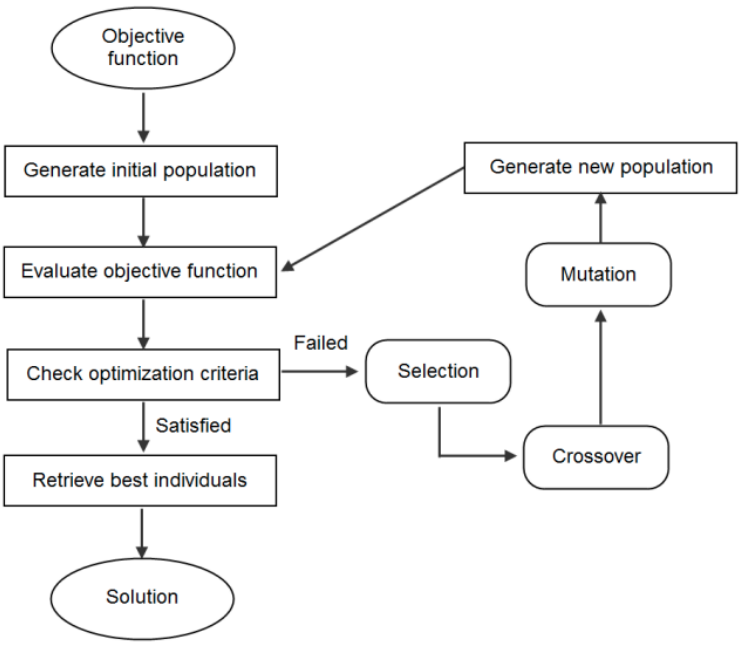

Figure 2. The general structure of evolutionary algorithms.

The wind farm layout optimisation problem can be formulated as finding $X = (x_1, \dots, x_B)$ to maximise $f(x)$ subject to boundary constraints $x_i^{(L)} \leq x_i \leq x_i^{(U)}, i = 1, \dots B$, where $f(X)$ is the maximum power output of the wind farm, B is the number of turbines in the wind farm and $x_1, \dots, x_B$ is the location of each wind turbine. In order to solve this problem, the differential evolution algorithm is summarised in the pseudocode shown in below.

1. Find a random suitable solution for the problems (initial population):

$\boldsymbol{P_0 = x_{j,i,0} = rand_j[0,1]\left(x_j^{(U)} - x_j^{(L)}\right) + x_j^{(L)}, j = 1, \dots, B, i = 1, \dots, NP,}$ where $\boldsymbol{rand[0,1]}$ is a uniformly generated random number between 0 and 1, NP is the size of the population and P_g is the population of generation g.

2. Evaluate the objective function (maximum power output of the wind farm) for the initial population using the depth-averaged CFD-based method.
3. Mutation: for every individual generate a trial parameter vector by crossing the

target vector with a noisy vector. A noisy vector can be obtained by randomly selecting three individuals $r_1, r_2, r_3 \in 1, \dots, NP, r_1 \neq r_2 \neq r_3$ and adding the weighted difference vector between the last two of them to the first one so that:

$$v_{j,i,g} = x_{j,r_3,g} + F\left(x_{j,r_1,g} - x_{j,r_2,g}\right),$$

where $F \in (0,1+]$, is the scale factor, $i = 1, \dots, NP$ and $j = 1, \dots, B$.

4. Crossover: a trial vector is generated with the target vector as follows:

$$u_{j,i,g} = \begin{cases} v_{j,i,g} \; if \; rand_j[0,1) \leq CR \vee \; j = k, \\ x_{j,i,g} \; otherwise \end{cases}$$

where $k \in 1, \dots, B$ is a random parameter index, chosen once for each i, $CR \in [0,1]$ is the crossover probability.

5. Correcting boundary constraint violations: the calculated trial vector might violate boundary constraints, since the algorithm is able to advance outside the original initialisation range. Boundary constraint violations can be fixed, for example, as follows:

$$u_{j,i,g} = \begin{cases} 2x_j^{(L)} - u_{j,i,g} \; if \; u_{j,i,g} < x_j^{(L)} \\ 2x_j^{(U)} - u_{j,i,g} \; if \; \; u_{j,i,g} > x_j^{(U)} \\ u_{j,i,g} \; otherwise \end{cases}$$

6. Selection: the trial vector is selected for the next generation if it is equal or better than the target vector:

$$X_{i,g+1} = \begin{cases} U_{i,g} \; \; if \; f\left(U_{i,g}\right) > f(X_{i,j}) \\ X_{i,g \; otherwise} \end{cases}$$

7. Return the best solution in the final population if the final condition is satisfied. Otherwise, use the new generation for a further run of the algorithm and return to Step 3.

It is worth noting again that terrain topography and wind turbines are included in the depth-averaged model using UDFs. Only one mesh is required in x- and ydirections. Otherwise, pre-processing would have to be done for every individual, which would slow down the optimisation process considerably. In the beginning of optimisation algorithm, the initial population is found and 2D depth-averaged CFD modelling is carried out for every individual. The new population is generated during Steps 3-6 in the described algorithm. Matlab launches the CFD simulation during the optimisation process. The program defines the parameter values for one individual and Matlab generates a Fluent journal file and UDFs for the source terms of the governing equations. After that, ANSYS Fluent is invoked to calculate the wind farm velocity field. In conclusion, Matlab uses these results to find the objective function of each individual and restores the optimisation algorithm.

Results

Lillgrund wind farm simulations

The depth-averaged simulation of Lillgrund wind farm without layout optimisation was investigated in the beginning. These results are validated by the comparison against data obtained by Nilson et al. (2014). In this study the validation of the Actuator Disk method with measured production data was presented for Lillgrund wind farm. A comparison with a well-known wind farm is indicated in that the depth-averaged model is also able to determine the power of the various turbines, supporting its estimation procedure from the wind energy point of view.

Lillgrund wind farm is located in Sweden and consists of 48 wind turbines. Each turbine in the presented wind farm is given a grid name by using row letters A-H and column numbers 1-8 as shown in Figure 3. The wind farm is dense, because the turbines are close to each other with a spacing of 4.3 turbine diameters in the prevailing wind direction and 3.3 turbine diameters in the transverse. Due to the shallowness of the water, two turbines are missing in Row E inside the wind farm.

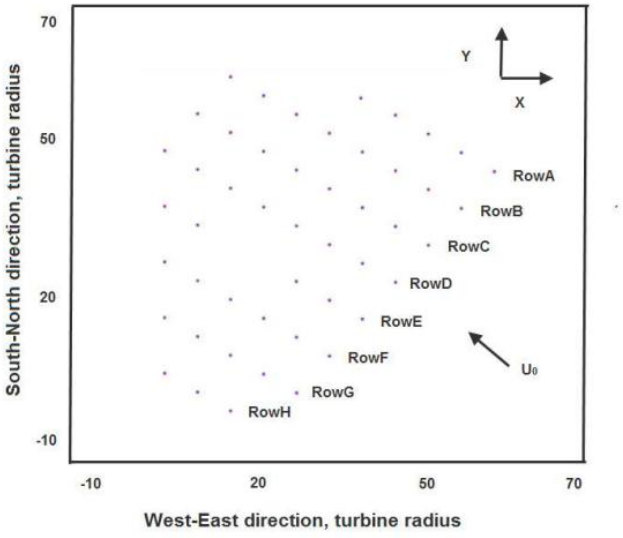

Figure 3. Layout of the Lillgrund wind farm (Nilson et al. (2014)).

The National Renewable Energy Laboratory (NREL) 5 MW turbine was used by Nilson et al. (2014). The turbine has a diameter of 93 m and a hub height of 65 m. The thrust coefficient of the NREL 5 MW turbine is equal to 0.812 and the power coefficient is 0.485. The inertial resistance factor C_2 for the depth-averaged method was found numerically and is equal to 0.121.

Only depth-averaged simulations of the 120 inflow angle were performed for different

turbulent intensities of 4%, 5.7% and 7.7% (Avramenko (2019)). In the depthaveraged method, the boundary conditions were periodic at the lateral boundaries, velocity inlet boundary conditions were used at the inlet and outflow boundary conditions were set at the outlet. The initial velocity is equal to 8.6 m/s.

Three meshes were used in depth-averaged simulations: the coarse mesh contains 30,967 quad elements, the reference mesh consists of 130,682 quad elements and the fine mesh uses 538,731 quad elements. The dependency of the power production, obtained from the depth-averaged simulation, in relation to grid resolution is analysed. The relative power of each turbine is the power of the turbine divided by the power of the first turbine in the row. The simulations are performed at 5.7% turbulence intensity (Figure 4).

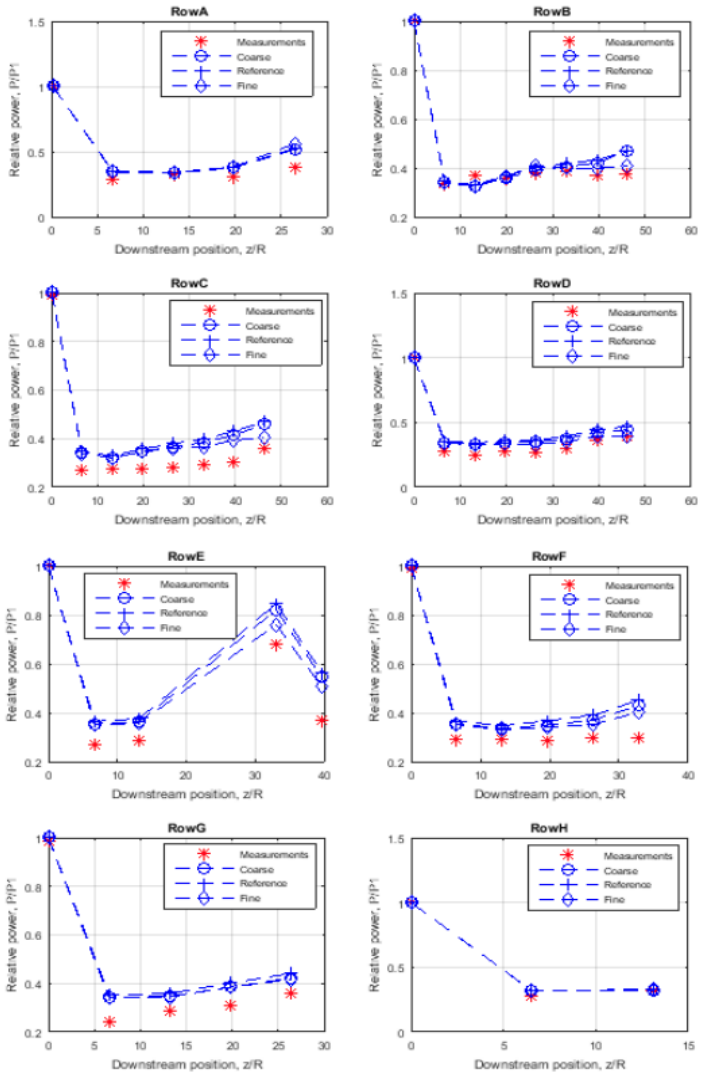

Figure 4. Effect on the relative power for the turbines in Row A-H by varying the mesh size.

The slight difference between meshes can be seen in Figure 4. The relative power of the turbines decreases slightly due to the increased mesh size and gets close to the measured values obtained by Nilson et al. (2014). The small difference between results obtained by reference and fine meshes also allows the use of the reference mesh in the following analysis due to the limitations of computational time.

Figure 5 shows the contour plot of the mean streamwise velocity from depthaveraged simulations using a reference mesh and 5.7% turbulence intensity. The relative power for Row A-H in the wind farm for different turbulent intensities is presented in Figure 6.

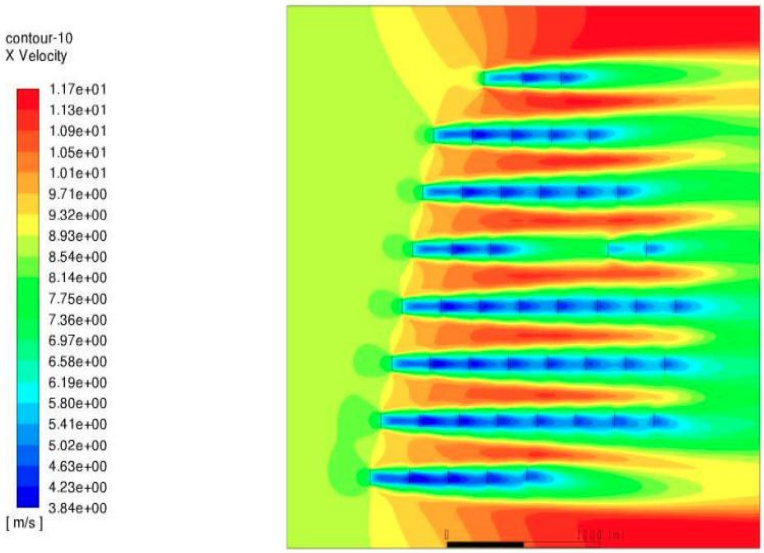

Figure 5. Mean streamwise velocity obtained from 2DDA simulation.

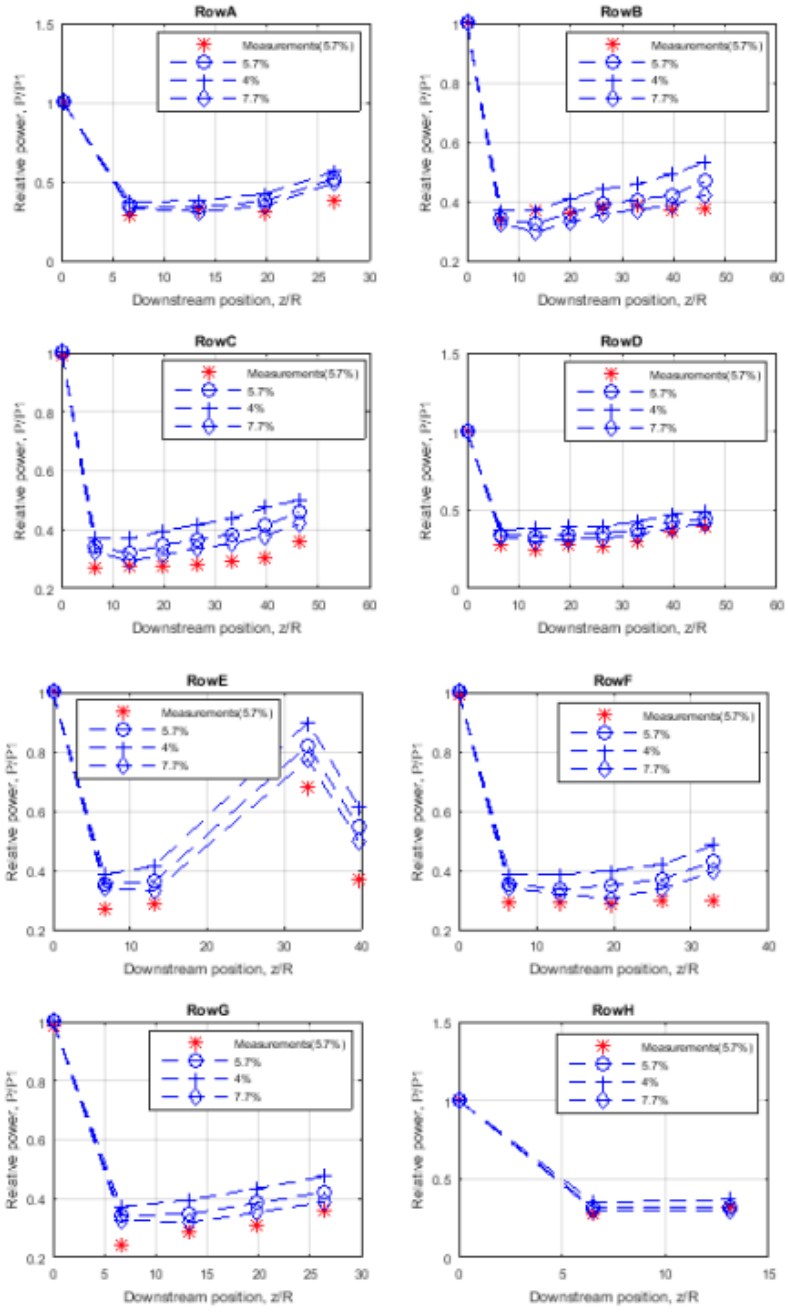

Figure 6. Relative power for Row A-H.

There is a slight difference for the turbines in the second row, and there is also a certain error behind the recovery gap. However, the depth-averaged simulation shows good agreement with measured data. Despite the limitations of the depth-averaged method,

the results demonstrate that this method predicts the wake behaviour quite accurately. For further optimisation, it is more important to obtain the right behaviour of the power production in the wind farm than the concrete values of the power production.

Layout optimisation Case Study

With a complex terrain simulation capability in place, two optimisation case studies on a Gaussian hill were processed. In the first case, the optimisation of several turbines (the number varies from one to five) was examined to confirm that the optimisation algorithm works accurately. The second case study concerns a layout optimisation on complex terrain with two different inflow directions for a wind farm containing five turbines.

The hill is described by

$$F(x,y) = He^{-\left(\frac{x^2}{2s_1^2}+\frac{y^2}{2s_2^2}\right)},$$

where $s_1 = 562, s_2 = 278$ and $H = 116$ m is the height of the hill. This topography is chosen because it is close to the real Askervein Hill located in Scotland (Figure 7). This hill has been widely investigated through field measurements, experiments and simulations by many researchers and is relatively isolated. Thus Askervein Hill is well-suited for our case study.

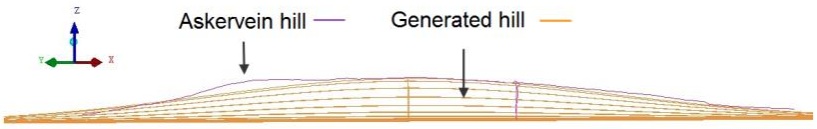

Figure 7. Topographic cross-sections through the hills.

The Nordtank NTK 500/41 wind turbine with LM 19.1 m was used in this work. The hub height of the turbine is 60 m and the diameter is 41 m. The turbine rotates at 27.1 rpm and generates 600 kW maximally. The power coefficient and power distribution were investigated by Mikkelsen (2003). 3D and depth-averaged numerical simulations of the Nordtank NTK 500/41 wind turbine on a Gaussian hill, described above, were considered by Avramenko (2019). The results show that the depth-averaged modelling saves computational resources and is accurate for the velocity calculations. The inertial resistance factor for the Nordtank NTK 500/41 wind turbine for depth-averaged simulation was found numerically by comparing the velocity from 3D and depth-

averaged numerical modelling, and it was equal to 0.11. The depth-averaged simulation was performed using a domain of 801 × 801 elements with dimensions of 8,000 m × 8,000 m (wind direction and cross-wind direction). The velocity in the inlet region was set at 15.2 m/s.

Single-objective optimisation is accomplished by using the differential evolution algorithm where the number of generations is 50, the number of individuals is 30, crossover probability is 0.9 and the scale factor is 0.9. The following constraints are used in the optimisation algorithm: the fixed number of wind turbines, the minimum distance between the turbines, the maximum acceptable power output, the boundary constraint violations. The minimum acceptable distance between the turbines is 2.5DM. The power output is limited to 600 kW for each turbine. The boundary box constraints are described by the following expression $-2000 < x < 2000, -2000 < y < 2000$ m. The point corresponding to the centre of the Gaussian hill is $x = 0, y = 0$.

In order to verify the optimisation algorithm, the layout optimisation of a wind farm containing one turbine, when the wind blows from the west, is carried out. With a single inflow direction, the optimal placement of the turbine would simply be on top of the hill to take full advantage of the higher wind speed. Figure 10 shows the initial population, the $15^{th}, 30^{th}$ and 50^{th} generations, obtained during the optimisation process.

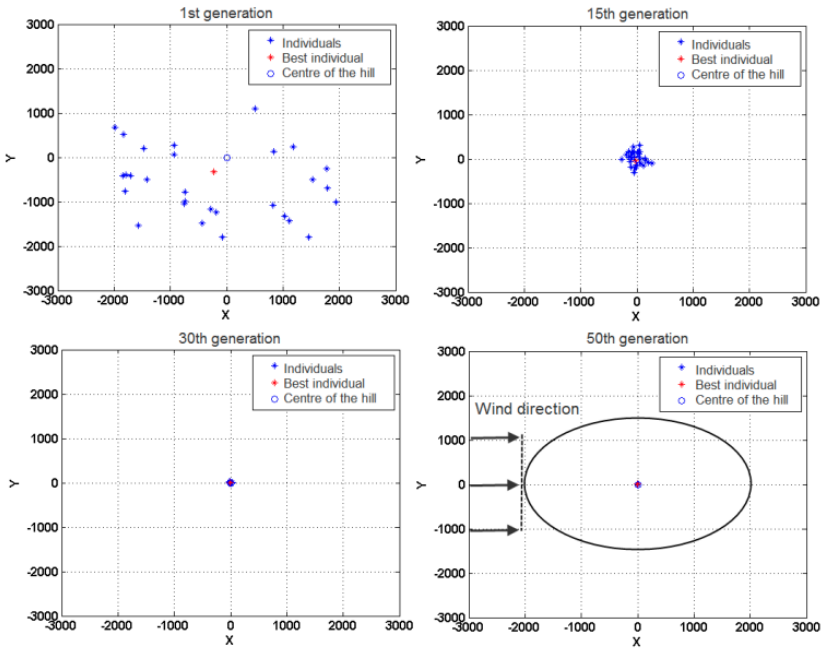

Figure 10. One turbine on a Gaussian hill: the 1st, 15th, 30th and 50th generations.

Hereinafter, the individual should only be considered as one layout of the wind farm. In Figure 10, the red star represents the best individual in the current population and the blue stars denote other individuals, with the circle being the top of the hill. Evolution is observed by comparing different generations to each other. Every individual in the population has almost the same location in the 50^{th} generation. Thus, the optimisation algorithm is converged to a single optimum.

The best layout was validated by comparing the 3D simulation for the initial and final layouts. The horizontal and vertical extents of the domain are 8000 m × 8000 m × 1200 m in 3D simulations. The centre point of the ground and the hilltop are located at x = 0, y = 0. A symmetry boundary condition is set on the top surface of the domain. The north and south boundaries of the computational domain are set as the periodic boundaries. The outflow boundary condition is used in the outlet. The inlet velocity and turbulence profiles are the same as those of Montavon (1998) and given by

$$u = \frac{u_*}{K} ln \frac{z}{z_0},$$

$$\epsilon = \frac{U_*^3}{hK\eta} e^{-\left(\frac{c}{1+c}+a\right)\frac{\eta^2}{2}},$$

$$\kappa = \sqrt{\frac{Kz}{C_\mu U_*}} \epsilon \left(\frac{U_*}{hK}\left[\frac{c}{\eta(\eta+c)} - \left(\frac{c}{1+c}+a\right)\eta + a\right]\right)^{-1/2},$$

where K is Karman's constant, $u_* = 0.654, z_0 = 0.03, B = 7.91, c = 0.183, \eta = {}^{z}/_{h}, h = 1090, a = {}^{1}/_{c}$.

The wind turbine is modelled in 3D simulation using the Actuator Disc method. The inertial resistance factor is 0.6136 and the thickness of the turbine can be taken as 1 m (Avramenko (2019)). The depth-averaged velocity in the 3D case is calculated by integrating the velocity profile over the depth of the channel. The depth of the channel in this case is calculated as $D(x, y) = 1200 - F(x, y)$, where $F(x, y)$ is represented by Equation 19. Figure 8 presents the vertical profiles of the mean streamwise velocity downstream of the turbine, located on the top of the hill. According to this figure, after the point has been reached where the maximum velocity deficit occurs, the wake begins to recover at a comparatively normal recovery rate. The rate of the wake recovery decreases considerably as we go further downstream. Figure 9 shows the profile of X velocity for the horizontal plane at the hub height for the 3D simulation (top) and the profile of the depth-averaged velocity obtained from the 2D depth-averaged simulation (bottom).

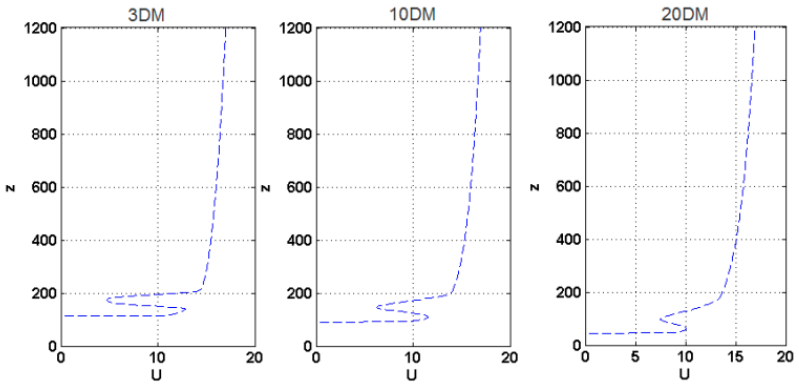

Figure 8. Vertical profiles of mean streamwise velocity downstream of the porous disc at x = 3DM, x=10DM and x=20DM, where DM is diameter of the turbine.

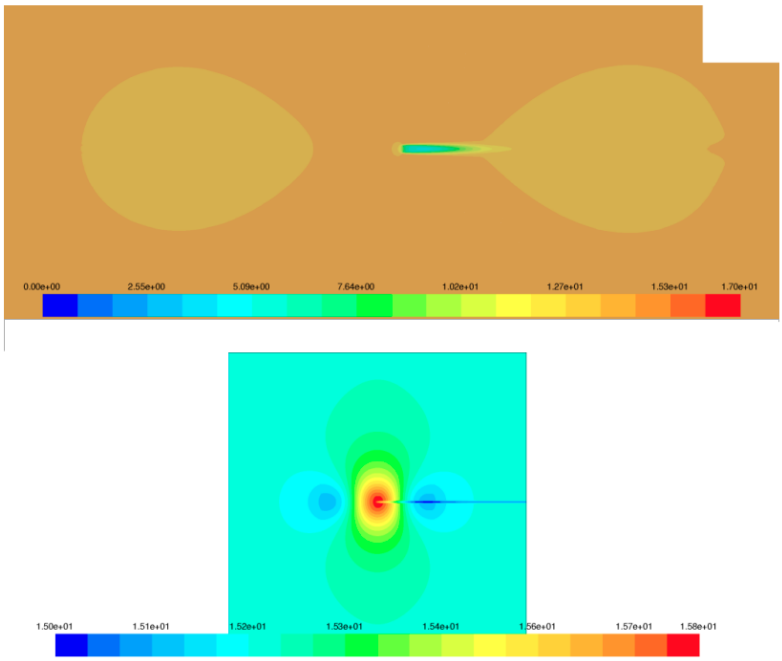

Figure 9. X velocity profile for the horizontal plane at the hub height for 3D simulation (top) and velocity profile obtained from 2D depth-averaged simulation (bottom).

The output power increases by 3.08% in 3D modelling. Figure 11 shows the power increase of 2.92% in the case of depth-averaged modelling.

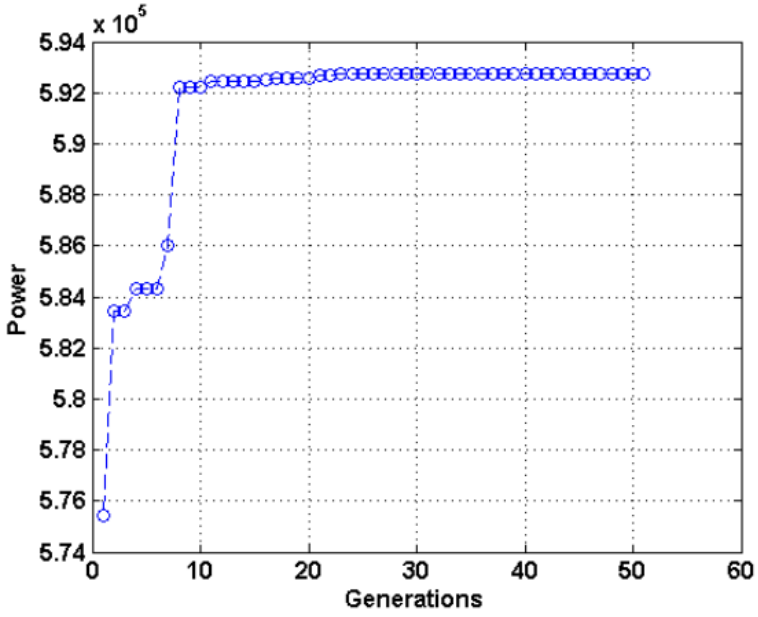

Figure 11. One turbine on a Gaussian hill: the relationship between the power and generations.

Then, the number of turbine in the wind farm is increased by two. It is worth noting that the mesh for the depth-averaged modelling is similar to the previous case. The mesh does not rebuild in the case of a change in terrain topography or the number of turbines, because all these changes are added to the governing equations by using UDFs. This is the main advantage of the depth-averaged approach in addition to the decrease of computational time. The results for this case are presented in Figure 12. The best individuals in the last population are located along the y-axis at approximately the same distance from the centre of the hill. The best wind farm layout provides the growth in power output compared to the initial geometry of 4.59%, as shown in Figure 13.

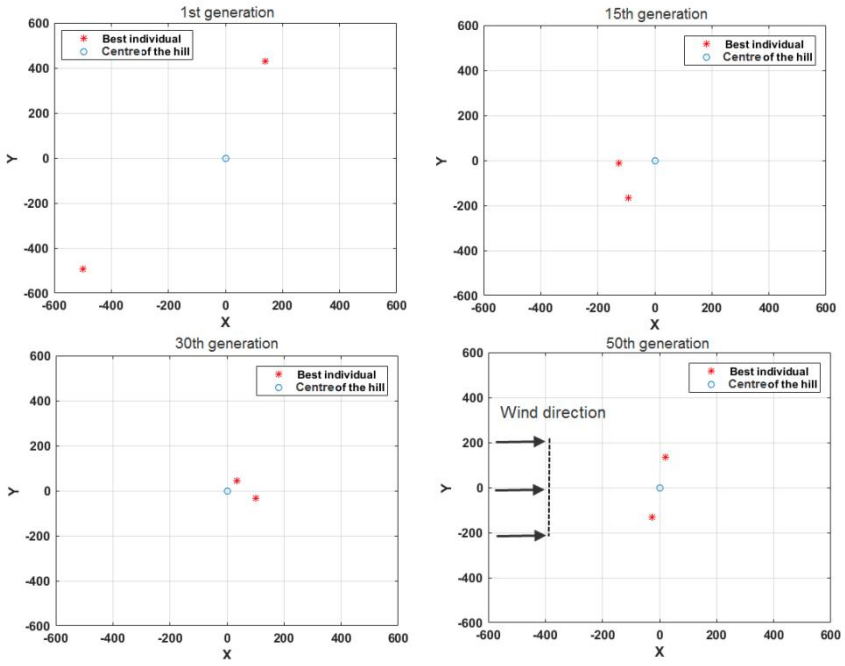

Figure 12. Two turbines on a Gaussian hill: the 1st, 15th, 30th and 50th generations.

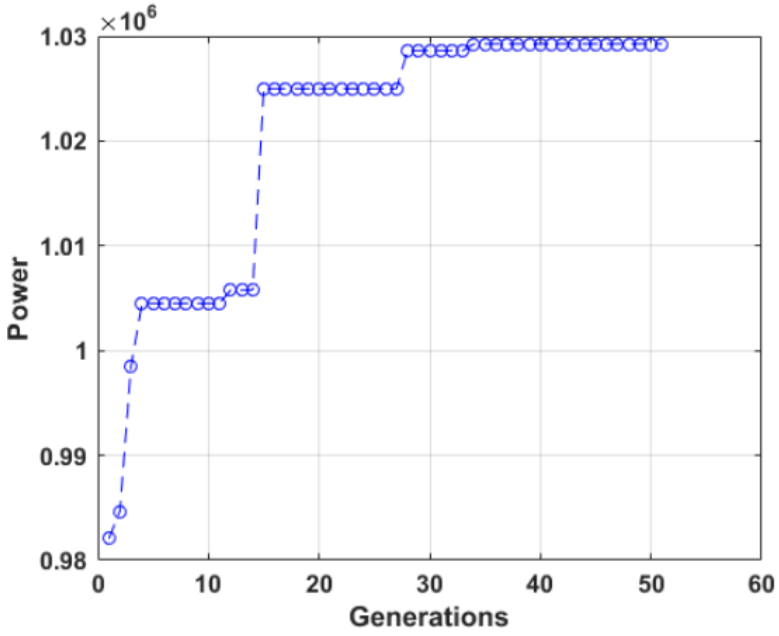

Figure 13. Two turbines on a Gaussian hill: the relationship between the power and generations.

Ideally, the wind rose for the presented landscape should be considered during optimisation process because the wind direction changes a lot over time. The wind rose presents the frequencies of the wind coming from different directions over a defined time period. The length of each line corresponds to the frequency that the wind blows per unit of time from a particular direction. A graphic of the wind rose may also include information about wind speed ranges. In this case, each line is divided into colour-coded bands that show the ranges of the wind speed. For this purpose, the cost function can be defined as

$$P = \sum_{i=1}^{n} \omega(i) P_i$$

Where P_i is the total power of the wind farm, calculated for the i th wind direction and speed, $\omega(i)$ denotes the frequency that is expected for each wind speed class corresponding to the i th wind direction and n is the number of wind directions. The wind turbines are automatically oriented to take maximum advantage of the kinetic energy of the wind. If the several wind directions are considered in wind farm optimisation, the turbine orientation has to be changed for each wind direction. In 3D simulation this implies a mesh rebuild, but in 2D depth-averaged simulation it can be done easily and may be regarded as another advantage of the depth-averaged method.

In this case, optimisation involves over two wind inflow directions with a wind speed of 15.2 m/s. In reality, Askervein Hill is oriented at an angle of 133° counter-clockwise from the east and the main wind directions are from the west and south, obtained from the wind rose (Stangroom (2003)). Here, the hill is oriented along the x-axis, but the wind blows from 227° and 317° east to keep the correct wind direction relative to the hill. Three different wind regimes were selected (227° , 317° from the east, and from both of these directions with frequencies of 56% and 44%) and optimal layouts were obtained for each regime (see Figures 14-15).

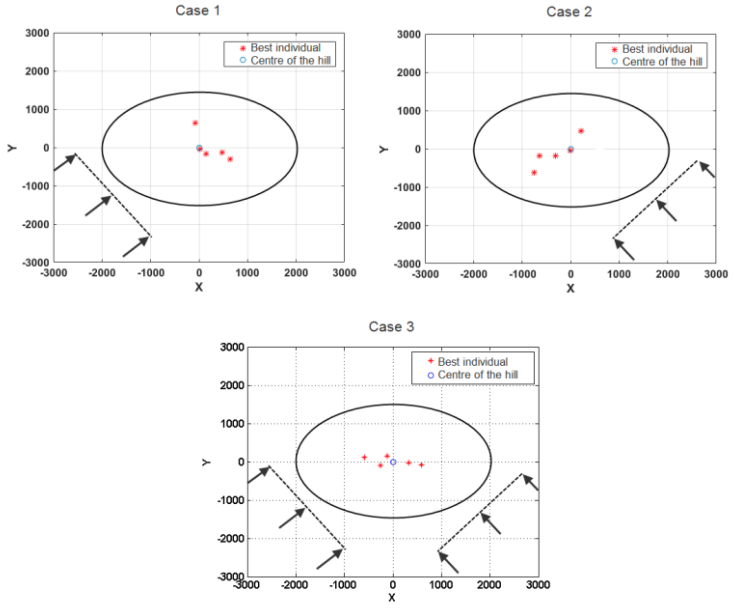

Figure 14. Five turbines on a Gaussian hill: the 1st, 15th, 30th and 50th generations for different regimes.

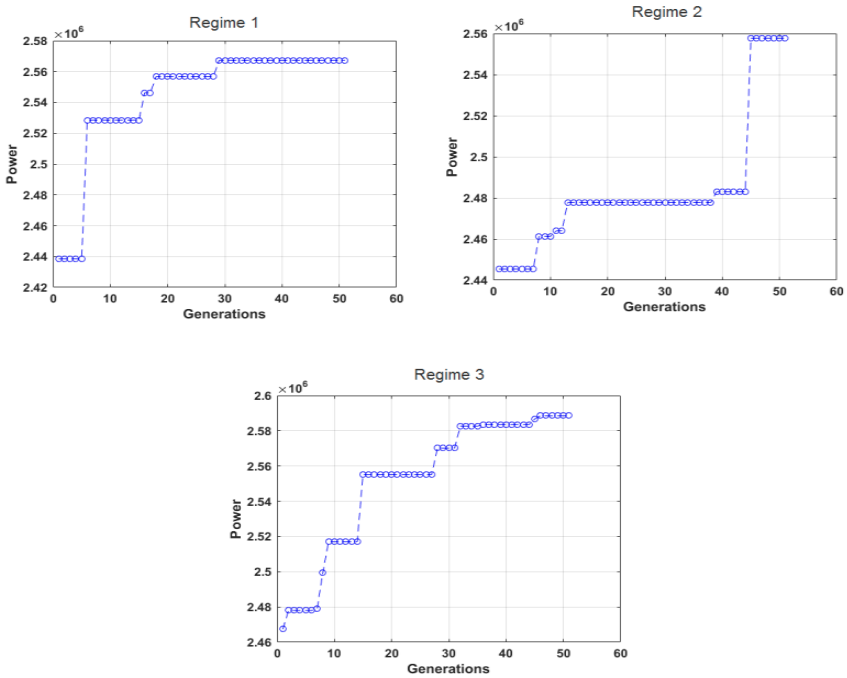

Figure 15. Five turbines on a Gaussian hill: the relationship between the power and generations for different regimes.

The power output is increased by 5.02% for the first regime, 4.39% for the second regime and 4.68% in the third regime when compared to the power output calculated for the initial layouts. These examples demonstrate that the depth-averaged method produces layouts that can compete with other optimisation algorithms in comparable conditions and outperforms optimisation with full 3D simulations.

Conclusions

Complex terrain has a substantial impact on the flow field within a wind farm and a substantial impact on layout optimisation results. The depth-averaged method was presented to simulate flow on complex terrain and subsequently combined with the optimisation algorithm. The terrain topography and wind turbines are included in the governing equations via the source terms. This method was validated by comparison against measured data from Lillgrund wind farm. Next, two layout optimisation studies were performed on a simplified model of Askervein Hill in Scotland. The first study confirmed that the optimisation algorithm correctly accounts for terrain effects and wind turbines in depth-averaged simulation. In our second study, five wind turbines and two inflow wind directions with different frequencies were considered. These layout optimisation results yield an improvement of almost 5% in our objective function relative to the starting configuration of the wind farm layout.

The main advantage of the presented method is its fast reaction to the variations of the complex terrain and the number of turbines. Complicated pre-processing work of the geometry and mesh generation can be ignored. This method uses a 2D mesh and therefore depth-averaged simulation is much faster. However, the depth-averaged approach also has its disadvantages. Firstly, the problem lies in the calculation of the inertial resistance factor, where the parameter could only be found numerically. Secondly, only the velocity field is calculated accurately during depth-averaged simulation. Other flow characteristics such as pressure, turbulence quantities, etc. are not the focus of this work. However, the results show that the depth-averaged approach could be a useful tool for wind farm designers, and it could be used as an optimisation tool during the design phase.

These depth-averaged simulation and optimisation results open many new paths for future research on wind farm performance on complex terrain. Further research on optimisation of larger wind farms and the consideration of the additional inflow directions and speeds to complete a full annual energy production optimisation are needed. Since evolutionary optimisation methods find local minima but are not guaranteed to reach the global minimum, future studies are needed to assess the impact of multiple restart strategies on the optimisation result.

Acknowledgements

We would like to thank the Academy of Finland for funding this research. We want to express our gratitude to IT u of Science in Finland (CSC) for their technical support that made this project possible. The authors are grateful to our colleagues from Peter

the Great St. Petersburg Polytechnic University, especially Evgeny Petukhov, for helping with the practical aspects of the optimisation algorithm.

References

[1] Allen, J., King, R., and Barter, G., 2019, "Wind farm simulation and layout optimization in complex terrain", Technical report, National Renewable Energy Laboratory, North American Wind Energy Academy.

[2] Amarala, L. and Castro, R., 2017, "Offshore wind farm layout optimization regarding wake effects and electrical losses", Engineering Applications of Artificial Intelligence, 60, pp. 26–34.

[3] Avramenko, A., 2019, "CFD-based optimization for wind turbine locations in a wind park", LUT University Press, Lappeenranta, Finland, ISBN 978-952-335-366-4.

[4] Brillard, A., 1986–1987, "Asymptotic analysis of incompressible and viscous fluid flow through porous media. brinkman's law via epi-convergence methods", Annales de la Faculte des sciences de Toulouse : Mathematiques, 8(5), pp. 225–252.

[5] Conan, B., Chaudhari, A., Aubrun, S., Hamalainen, J., and Hellsten, A., 2016, "Boundary-layer meteorology experimental and numerical modelling of flow over complex terrain: The bolund hill", Boundary-Layer Meteorology, 158(2), pp. 183–208.

[6] Feng, J., Shen, W., and Li, E. 2018, "An optimization framework for wind farm design in complex terrain. Applied Sciences", 18(11) pp. 2053–2053.

[7] Gao, X., Yang, H., and Lu, L. 2014, "Study on offshore wind power potential and wind farm optimization in hong kong", Applied Energy, 130, pp. 519–531.

[8] Gonzalez, J., Payan, M., Santos, J., and Gonzalez-Longatt, F., 2014, "A review and recent developments in the optimal wind turbine micro-siting problem", Renewable and Sustainable Energy Reviews, 30, pp. 133–144.

[9] Hamalainen, J., Tiihonen, T., Madetoja, E., and Ruotsalainen, H., 2008, "Cfd-based optimization for a complete industrial process: Papermaking", Optimization and Computational Fluid Dynamics, pp. 267–289.

[10] King, R., Dykes, K., Graf, P., and Hamlington, P., 2017, "Optimization of wind plant layouts using an adjoint approach", Wind Energy Science, 2, pp. 115–131.

[11] Kuo, J., Romero, D., Beck, C., and Amon, C., 2016, "Wind farm layout optimization on complex terrains - integrating a cfd wake model with mixed-integer programming", Applied Energy, 178, pp. 404–414.

[12] Landberg, L., Myllerup, L., Rathmann, O., and Petersen, E., 2003, "Wind resource estimation an overview", Wind Energy, 6, pp. 261–271.

[13] Lyytikainen, M., Hamalainen, T., and Hamalainen, J., 2009, "A fast modelling tool for plate heat exchangers based on depth-averaged equations", International Journal of Heat and Mass Transfer, 52(5–6), pp. 1132–1137.

[14] Mikkelsen, R., 2003, "Actuator Disc Methods Applied to Wind Turbines", Technical University of Denmark, Lyngby, Denmark, ISBN 87-7475-296-0.

[15] Montavon, C., 1998, "Simulation of Atmospheric Flows over Complex Terrain

for Wind Power Potential Assessment", Lausanne, EPFL.

[16] Nilson, K., Ivanell, S., Hansen, K., Mikkelsen, R., Sørensen, J., Breton, S., and Henningson, D., 2014, "Large-eddy simulations of the lillgrund wind farm", Wind Energy, 18, pp. 449–467.

[17] Osuna-Enciso, V., Espinoza-Haro, J., Oliva, D., and Hernandez-Ahuactzi, I., 2018, "Offshore wind farm layout optimization via differential evolution", Computacion y Sistemas, 22(3).

[18] Park, J. and Law, K., 2015, "Layout optimization for maximizing wind farm power production using sequential convex programming", Applied Energy, 151, pp. 320–334.

[19] Politis, E., Prospathopoulos, J., Cabezon, D., Hansen, K., Chaviaropoulos, P., and Barthelmie, R., 2012, "Modeling wake effects in large wind farms in complex terrain: the problem, the methods and the issues", Wind Energy, 15(1), pp. 161–182.

[20] Queney, P., 1947, "The problem of air flow over mountains: A summary of theoretical studies", Bulletin of the American Meteorological Society, 29(1), pp. 16–26.

[21] Rastogi, A. and Rodi, W., 1978, "Predictions of heat and mass transfer in open channels", Journal of the Hydraulics Division, (HY3), pp. 397–420.

[22] Rodi, W., 1984, "Turbulence Models and Their Application in Hydraulics - A State of the Art Review", Ashgate Pub Co.

[23] Sessarego, M., Shen, W., Laan, M., Hansen, K., and Zhu, W., 2018, "Cfd simulations of flows in a wind farm in complex terrain and comparisons to measurements", Applied Sciences, 8(5).

[24] Stangroom, P., 2003, "CFD modelling of wind flow over terrain", University of Nottingham, Nottingham, United Kingdom.

[25] Turner, S., Romero, D., Zhang, P., Amon, C., and Chan, T., 2014, "A new mathematical programming approach to optimize wind farm layouts", Renewable Energy, 63, pp. 674–680.

[26] Wood, N., 2000, "Wind flow over complex terrain: A historical perspective and the prospect for large-eddy modelling", Boundary-Layer Meteorology, 96(1), pp. 11–32.